Materials Today: Proceedings 38 (2021) 1183–1190

Contents lists available at ScienceDirect

Materials Today: Proceedings

journal homepage: www.elsevier.com/locate/matpr

Modified nanostructured titania photocatalysts for aquatic disinfection applications

David Dodoo-Arhin [a,b,*], Elsie Bowen-Dodoo [a,b], Benjamin Agyei-Tuffour [a], Emmanuel Nyankson [a], John D. Obayemi [c], Ali A. Salifu [c], Abu Yaya [a], Henry Agbe [d], Winston O. Soboyejo [c]

[a] Department of Materials Science & Engineering, University of Ghana, P.O. Box LG 77, Legon-Accra, Ghana
[b] African Materials Science and Engineering Network (A Carnegie-IAS RISE Network), South Africa
[c] Department of Mechanical Engineering, Worcester Polytechnic Institute (WPI), Worcester, MA, USA
[d] Centre Universitaire de Recherche sur l'Aluminium, Université du Québec à Chicoutimi, Québec G7H 2B1, Canada

ARTICLE INFO

Article history:
Received 5 July 2020
Received in revised form 27 July 2020
Accepted 31 July 2020
Available online 18 September 2020

Keywords:
Photocatalysis
TiO_2
Sol-gel
Escherichia coli
Water Treatment
Reactive Oxygen Species

ABSTRACT

According to the SDG 6, everyone on earth should have access to safe and affordable drinking water. In sharing water-treatment technologies that leads to accomplishing this goal, it is imperative to devise ways of removing microbial contaminants such as E. coli from drinking water especially in resource-limited settings that lack centralized water supply systems. One of the approaches is bacterial disinfection of water at the point of use. In this study, the bactericidal effects of the photocatalysis of titanium dioxide-based nanoparticles under UV and visible light are explored.

Pristine and silver doped nanostructured mesoporous titanium dioxide (Ag-TiO_2, TiO_2) particles with high specific surface area and average crystallite domain size of ~ 7.0–7.5 nm were prepared using the simple and cost effective sol–gel technique followed by thermal treatment. The addition of Ag^+ ions during the hydrolysis/condensation of the $Ti^{(IV)}$ molecular precursor led to homogeneous dispersion of the Ag^+ cations on the titania matrix. The As-prepared nanoparticles were characterized using X-Ray Diffraction (XRD), Brunauer–Emmett–Teller (BET) surface area analysis, Transmission Electron Microscopy (TEM), Scanning Electron Microscopy (SEM), thermogravimetry, Fourier Transform Infra-Red (FTIR), and Raman Spectroscopy. X-ray diffraction, FTIR and Raman spectroscopy confirmed that the crystalline structure of the TiO_2 matrix corresponds to the anatase polymorph; however, the presence of the dopant led to an increase in the system disorder due to the rise in concentration of oxygen vacancies. The As-prepared nanoparticles were used for *Escherichia coli* (E. coli) inactivation under dark and UV–Visible light conditions. Under dark conditions, Ag doped titania and pristine titania resulted in ~ 95% and ~ 64% E. coli population inactivity while under light conditions, ~99% and ~ 97% degradation respectively were observed. Taken together, these results demonstrate that, the synthesized TiO_2 nanoparticles have promising applications in the light mediated point of use inactivation of bacterial contaminants in water.

Selection and peer-review under responsibility of the scientific committee of the International Symposium on Nanostructured, Nanoengineered and Advanced Materials.

1. Introduction

Many developing countries are still struggling with improving water security [1] According to the World Health Organization (WHO), 3.4 million people die annually from being exposed to waterborne diseases, which are preventable health issues [2]. Unsafe drinking water poses health risks through transmission of diseases like cholera, diarrhoea, typhoid, ascariasis and dysentery [3]. The presence of E. coli in water indicates human or animal waste contamination [4]. E. coli is the cause of many bacterial infections and it accompanies underlying ill-health symptoms such as cramps, diarrhoea, nausea etc.

Many techniques have been put in place to provide safe drinking water right from the point of use (POU) [5], especially in underdeveloped areas where centralized water supply systems

* Corresponding author.
E-mail address: ddodoo-arhin@ug.edu.gh (D. Dodoo-Arhin).

https://doi.org/10.1016/j.matpr.2020.07.710
2214-7853/
Selection and peer-review under responsibility of the scientific committee of the International Symposium on Nanostructured, Nanoengineered and Advanced Materials.

are non-existent [6]. These methods include chlorination, ceramic filtration and solar water disinfection (SODIS) [5]. There are new alternatives to the above water disinfection methods. The use of advanced oxidation processes (AOPs) is currently being employed for the removal of both organic and inorganic pollutants [7]. The underlying principle here is that there is oxidation of highly reactive oxygen species (ROS) such as hydroxyl (OH) radicals and these are what degrade the contaminants. AOPs in some cases are carried out with a combination of a catalyst and light. This process is termed photocatalysis [7]. Recent studies show that TiO_2 nanoparticles are very effective in bacteria inactivation due to their high photocatalytic activity [8,9].

Nanocrystalline materials have been studied extensively because of the unique properties that they possess at that nanoscale and they find use in various fields of research. Metal oxides are probably the most common of these nanomaterials, owing to their structural, physical and chemical properties, which may be tuned by manipulation of their band gaps [10]. TiO_2 is an advanced nanoceramic material [11] and its discovery as an active photocatalyst in 1972 is credited to Fujishima and Honda [7,12]. This naturally occurring oxide has a wide range of industrial and daily life applications which include photocatalytic environmental remediation procedures, gas sensors, pigments in paint, bacterial decontamination, cleaning agent components etc. Sustained interest in TiO_2 nanoparticles is due to their excellent photocatalytic properties such as low cost, high chemical stability, non-toxicity, insolubility in water and resistance to most chemicals [12,13]. The wide band gap of TiO_2 which is $\sim$ 3.2 eV, limits its photocatalytic activity to the UV range which only constitutes $\sim$ 4–5% of the solar spectrum [13–15]. To increase the light harvest capabilities, it is necessary to extend absorption to the visible and near-infra-red spectral region which accounts for $\sim$ 40% of solar spectrum [9]. Visible light active (VLA) photocatalysis is an area of interest for disinfection applications and may be achieved through transition metal doping of TiO_2 material [14,15].

In addition, silver (Ag) is well known for its bactericidal properties [14,16]. Mechanisms of antibacterial effect of silver are still under investigation; however multiple pathways such as binding of Ag^+ ion with the negatively charged peptidoglycan cell wall and the ROS-mediated oxidative stresses, leading to bacterial cell death have been implicated [17]. Prior studies report strong photocatalytic activity when Ag is incorporated into the structure of TiO_2. Enhanced photocatalytic activity may be attributed to electron-hole separation via electron trapping, shifting of the absorption spectrum to a longer wavelength in the visible region and modification of photocatalyst surface [14]. Also, the high surface area and small crystal size of TiO_2 make it a suitable metal oxide candidate for doping with silver nanoparticles [18]. Ag doped TiO_2 nanoparticles have found use in water purification applications. In this work, pristine TiO_2 and Ag doped TiO_2 were synthesized using the sol–gel method. The photocatalysts were characterized using X-ray Diffraction, Fourier Transform Infrared spectroscopy, Thermogravimetric Analysis, Scanning Electron Microscopy, Transmission Electron Microscopy and Brunauer Emmett Teller (BET) analysis. The effect of TiO_2 and Ag-doped TiO_2 on E. coli cells under UV, visible light and dark conditions were also investigated.

2. Materials and methods

2.1. Materials

All reagents used in this study were of analytical grade and used without further purification. Titanium (IV) isopropoxide (TTIP) was provided by Arcos Organics. Silver nitrate ($AgNO_3$) and isopropanol were purchased from Fisher Chemicals. Absolute ethanol was obtained from Pharmco Products, Inc.

2.2. Preparation of photocatalysts

TiO_2 nanoparticles were synthesized using the sol–gel method adopted by Sakthivel et al. [19] while Ag-doped TiO_2 were by a method adopted by Ozimek et al. [20]. To synthesize TiO_2 nanoparticles, 25 ml of TTIP was added to 25 ml of absolute ethanol and stirred. This was then added to 100 ml of deionized water and stirred at 600 rpm for 3 h. The resulting sol was oven dried at 75 °C for 5 h, and then calcined at 450 °C in an electric furnace for 2 h at a ramping rate of 10 °C/min. Ag-doped TiO_2 nanoparticles were also prepared through sol–gel method. 54 ml of TTIP and 252 ml of isopropanol were mixed with 42 ml of deionized water to obtain a sol. The sol was stirred at room temperature for 2 h. 2.7 ml of 0.05 M $AgNO_3$ solution was added to the mixture and stirred for another 2 h. Oven drying, and then calcination, were carried out at 100 °C for 12 h and 450 °C for 2 h respectively.

2.3. Characterization of the photocatalysts

XRD was carried out using a Bruker D8 focus X-ray Diffractometer. Measurements were conducted in the 2θ range of 20° – 80° at a scan speed of 0.02°/s and step size of 0.05°, using Cu Kα (λ = 1.5406 Å) radiation. Surface functional groups were recorded on a Bruker Vertex 70 Fourier Transform Infrared (FTIR) spectrometer equipped with a Specac Golden Gate ATR accessory. Spectra data were recorded within the 4000–600 cm^{-1} spectral range in transmission mode and analyzed using Bruker's OPUS software. The structural properties were determined on a Technospex micro-Raman-532TEC-Ci spectrometer equipped with a μ-soft 2.0 analytical software in the spectral range of 100–3400 cm^{-1} and spectral resolution of 7 cm^{-1}. All the powder samples were analysed using a Cobolt excitation laser of 532 nm (with a laser power of 50 mW) through an X50 objective piece and an acquisition time of 120 s. Thermal analysis was conducted using a Netzsch TG 209 F1 Libra thermal analyzer. 10 mg of the specimen was placed in an alumina (Al_2O_3) crucible (100 mg capacity), subjected to a linear heating ramp between 15 °C and 800 °C at a rate of 10 °C/min and a cooling rate of 50 °C/min in an oxygen environment. The test measurements were made for the mass change (loss) of the sample as a function of the temperature and the phase changes by the adsorption or the emission of energy. Specific surface area measurements were conducted on a Quantachrome Autosorb IQ sorption analyzer using the multipoint Brunauer-Emmett-Teller (BET) standard technique. Prior to the measurements, samples were degassed under vacuum at 350 °C for 8 h in nitrogen atmosphere and an adsorbate at 77 K. Full isotherms were run between relative pressures of $4E^{-6}$ to 1. Morphological data of the prepared samples were analyzed using a JEOL-JSM 7000F scanning electron microscope equipped with EDAX-EDS and a Philips CM 10 transmission electron microscope.

2.4. Culturing of E.Coli

Escherichia coli (C-3000 strain, ATCC 15597) was grown in nutrient broth at 37 °C for 24 h in a shaker incubator (Model G25, New Brunswick Scientific, Edison, NJ) at 100 rpm to reach stationary growth phase. The stationary phase cultures were then centrifuged at 3000 rpm for 5 min to harvest the E. coli cells. Subsequently, the E. coli cells were re-suspended in 150 ml of 0.9% sterile saline solution in sterile conical flasks to prepare working E. coli suspensions containing approximately 10^6 to 10^7 colony forming units per ml (cfu/ml).

2.5. Bacteria photocatalytic degradation

0.2 g of the pristine and Ag-doped TiO_2 nanoparticles were added to separate flasks. The setup was kept in the dark and subjected to constant stirring at 500 rpm for about 30 min to attain equilibrium. Thereafter, the reactor flasks were either exposed to UV-A light (6-watt UV lamp, 259 nm) or visible light (7-watt LED table lamp) under constant stirring for 4 h, with 500 μl aliquots withdrawn at time 0 and at 1 h intervals to determine the bacteria concentration. Conical flasks containing only E. coli suspensions (without the TiO_2 nanoparticles) were also irradiated with UV-A and visible light under the same conditions as above, as controls. Another control experiment was set up to study the interaction of the TiO_2 nanoparticles with the E. coli cells. This was done by adding 0.2 g of the TiO_2 nanoparticles to the E. coli suspensions and treating the reactor flasks under the same conditions above but without the UV-A or visible light irradiation (i.e., under dark conditions).

At the predetermined time intervals, the concentrations of viable E. coli cells in the reactor flasks were determined by serial dilution with the 0.9% saline solution followed by the plating of 1 ml aliquots onto Petrifilm E. coli/coliform count plates (3 M, St Paul, MN, USA). After incubating the Petriflm plates at 37 °C for 24 h, the number of E. coli colonies on the plates were counted and expressed as the E. coli concentration in cfu/ml. The bacteria inactivation rate was calculated using the formula:

$$R\% = \left(\frac{C_o - C_t}{C_o}\right) \times 100 \quad (1)$$

where C_o is the initial bacteria concentration, C_t is bacteria concentration at time t and R % is the inactivation rate.

3. Results and discussion

3.1. XRD analysis

The X-ray diffraction profiles shown in Fig. 1 confirm the formation of anatase TiO_2 phase with tetragonal structure belonging to I41amd space group. Doping with Ag did little to change the crystallinity of pristine TiO_2. All peaks indexed, agree with database records for anatase phase of TiO_2 [19]. There was a slight increase in intensity in the Ag- doped TiO_2. The low loading of Ag precursor solution during synthesis led to a weak Ag characteristic diffraction peak around 2θ 31^0, which also suggests a good dispersion of the very small crystallite size Ag particles in the TiO_2 matrix [14]. The average crystallite sizes of the as-prepared titania nanoparticles as estimated using the Scherrer equation was found to be ~ 7.46 nm for Ag-doped TiO_2 and ~ 7.04 nm for pristine TiO_2.

3.2. FTIR and Raman spectroscopy

In the FTIR spectra shown in Fig. 2, the vibrational bands at 3250 cm^{-1} and 3350 cm^{-1} are characteristic of hydroxyl groups.

The peak at 2973 cm^{-1} in the Ag-doped TiO_2 could be associated with possible residual organic matter from alkoxide and solvent. Bands at 1636 cm^{-1} and 1640 cm^{-1} in TiO_2 and Ag-doped TiO_2 respectively, represent the stretching vibrations of titanium carboxylates. The Ag-doped TiO_2 revealed a peak at 1380 cm^{-1} which was absent in the TiO_2 spectrum. This peak is attributed to Ag and TiO_2 interactions and could result from the decomposition of $AgNO_3$ [21,14].

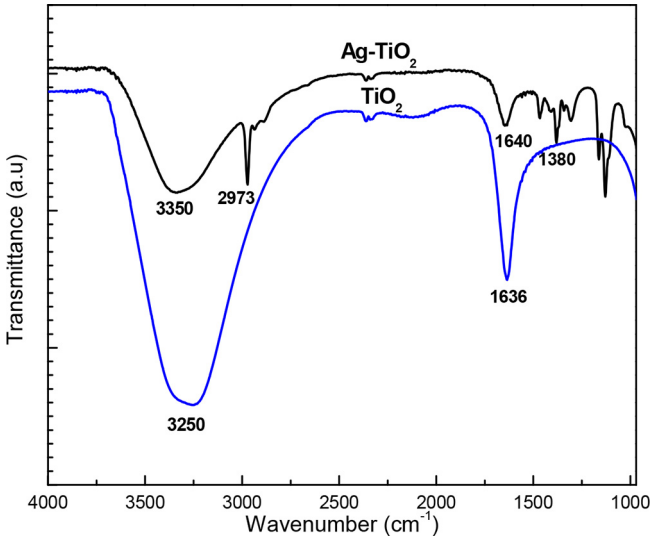

Fig. 2. FTIR spectra of As-prepared TiO_2 and Ag-doped TiO_2.

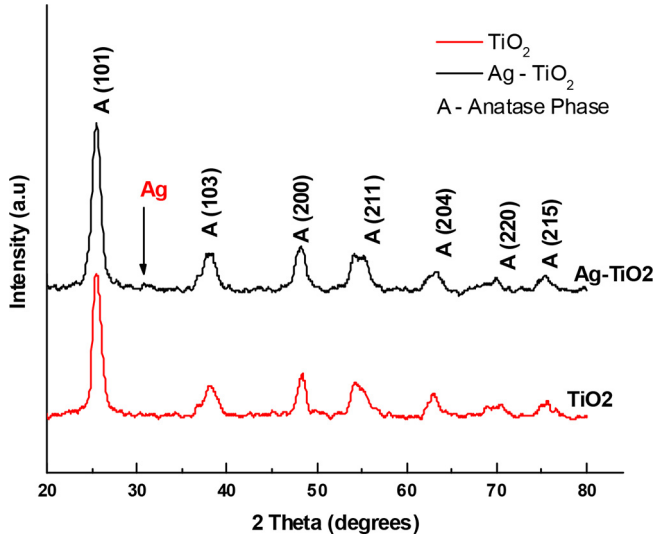

Fig. 1. XRD patterns of pristine TiO_2 and Ag-doped TiO_2.

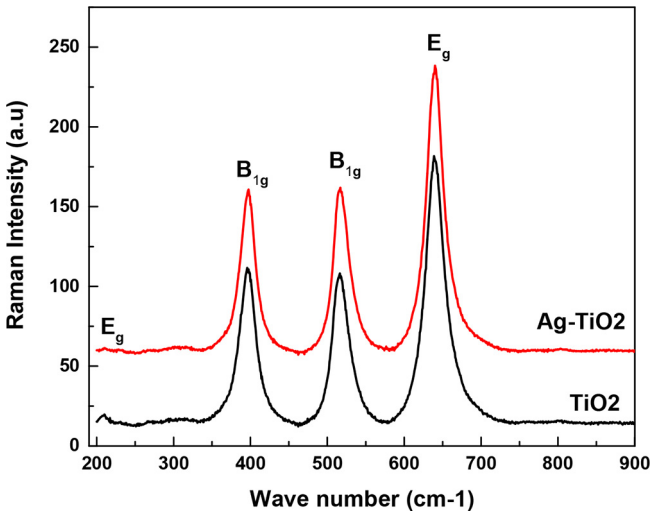

Fig. 3. Raman spectra of the TiO_2 photocatalysts.

The catalysts were also evaluated using Raman spectroscopy (Fig. 3). All samples exhibit typical anatase vibration modes ($A_{1g} + 2B_{1g} + 3E_g$), with the A_{1g} mode being overlapped with the B_{1g} peak around 537 cm^{-1} [22–25]. A slight shift in the signals and slightly broader peak was observed for the Ag-doped sample than for the undoped TiO_2 photocatalyst. This slight shift and broadening of the Raman-active band can be attributed to the concentration of oxygen vacancies on the photocatalysts, as previously shown by Parker and Siegel. [26–28] Thus, Raman analysis indicates that both undoped and Ag-doped TiO_2, exhibit an anatase crystalline structure; but the introduction of the dopant induces the formation of oxygen vacancies on the oxide surface, thereby increasing the system disorder.

3.3. Microscopy and surface area analysis

SEM micrographs of the TiO_2 nanoparticles obtained after calcination at 450 °C are shown in Fig. 4. The nanoparticles are seen to be highly agglomerated in both samples and there is an obvious decrease in particle size due to the Ag doping. The TiO_2 micrograph in Fig. 4(a) captures the well-defined spherical nature of the nanoparticles. The particles are generally homogeneous. The SEM image for the Ag-doped nanoparticles in Fig. 4(b) shows that doping did little to change the topography of the TiO_2 surface. The nanoparticles are irregularly shaped, containing aggregates of smaller crystals. It could also be said that silver particles were too tiny to be observed under the scanning electron microscope resolution used due to the high aggregation of nanoparticles. Fig. 5 (a) and (b) show images from TEM analysis with agglomeration in both samples. Particle size distribution is shown in Fig. 5 (c) and (d) with a range of ~ 9–18 nm for TiO_2 and a range of ~ 7–12 nm for Ag-doped TiO_2.

The nitrogen (N_2) sorption isotherms in Fig. 6 shows that, both isotherms for the Ag-TiO_2 and TiO_2 are of the type IV sorption isotherms. This is a confirmation of the formation of mesoporous nano-adsorbents according to the IUPAC classification [29]. The isotherms have the feature of type H-2 hysteresis loop but in both cases very narrow. For porous materials with this kind of hysteresis loop it tells of irregular pore size distribution and poorly defined pore shapes.

Surface areas for the two photocatalysts were found to be 129.7 m^2/g (TiO_2) and 109.8 m^2/g (Ag-TiO_2): a clear indication that Ag doping decreases the surface area.

3.4. Thermal analysis of photocatalysts

The thermal properties of the developed photocatalysts are shown in Fig. 7. For the pristine TiO_2, a region of mass loss of about 25% is recorded around 110 °C. This may be attributed to the loss of adsorbed water on the titania surfaces. For the Ag-doped TiO_2, a mass loss of around 18% is recorded between 25 °C and 180 °C. This area accounts for the loss of adsorbed water. A second region in the temperature range of 180 °C to 240 °C recorded a mass loss of ~ 6%. This may be attributed to the loss of organic matter from the sample. In all plots, from 250 °C to 600 °C, there is no mass loss recorded in the samples. This confirms thermal stability of the synthesized catalysts in that temperature range.

3.5. Bacteria photodegradation

3.5.1. Bacteria inactivation studies under UV irradiation

Fig. 8 (a) shows the inactivation rate of the photocatalysts on E. coli under UV-A condition. E. coli assay irradiated by UV was also investigated as a control to establish the population response to UV light. E. coli coliform in the control sample increased slightly, with a negative inactivation rate after 2 h. However, after 4 h, the rate increased to 7% indicating that UV light seemed to have an effect on the bacteria cells. Both pristine TiO_2 and Ag-TiO_2 exerted high bacterial inactivation rates throughout the experiment with the Ag-doped photocatalyst exhibiting ~ 99% inactivation after just 2 h and maintaining this rate after 4 h. TiO_2 exhibited ~ 99% inactivation after 3 h slightly reducing to ~ 97% inactivation after 4 h.

The mechanism behind the inactivation by the photocatalysts and exposure to UV is attributed to the formation of ROS [8,30]. In the presence of UV, reactive species generated at the titania surface-induced oxidative stresses on the bacteria, leading to DNA damage in the cells [30]. UV light has been used in many sterilization applications. DNA molecules are known to absorb UV photons between wavelengths of 200 and 300 nm. Maximum absorption occurs around 260 nm. Short wavelength UV

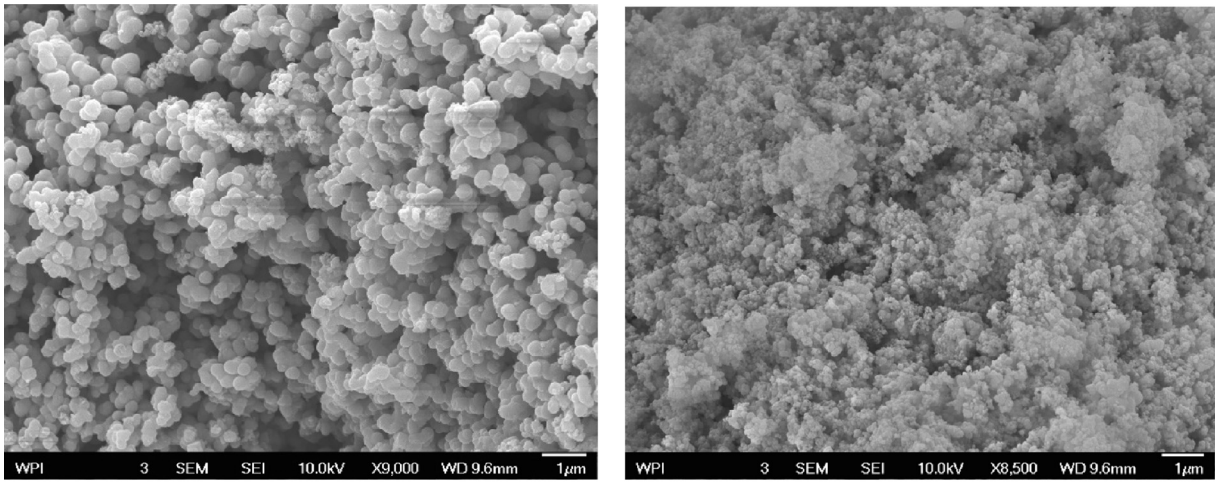

Fig. 4. SEM results of (a) TiO_2 and (b) Ag-TiO_2.

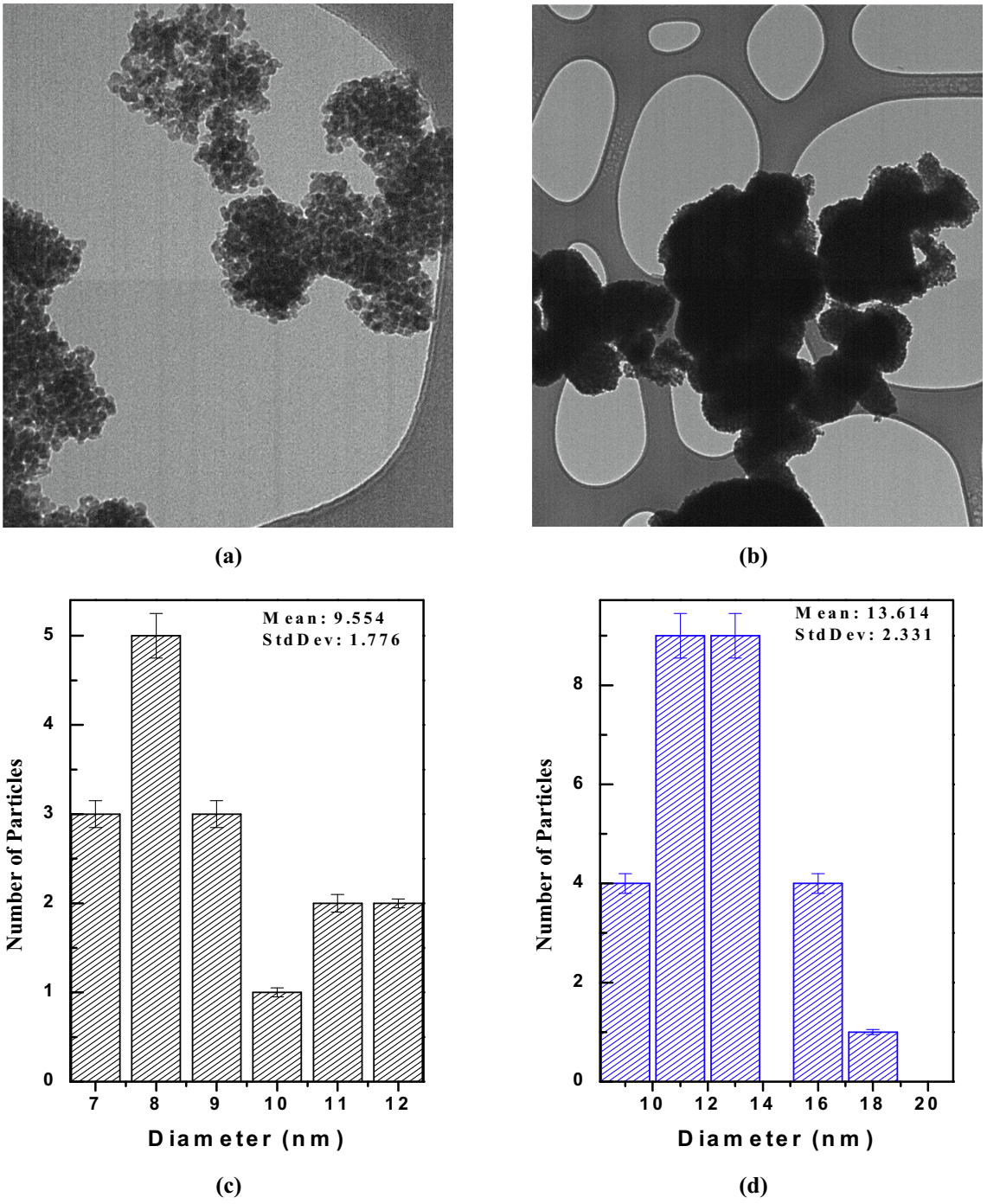

Fig. 5. TEM of calcined (a) Ag doped TiO_2, (b) pristine TiO_2, and Particle size distribution of (c) Ag doped TiO_2, (d) pristine TiO_2.

light can also break O–H, P–O, and N–H, bonds and result in the formation of energetic free radicals. Once again, damage to the DNA cells leading to changes in DNA strand is the likely factor for E. coli inactivation. Death follows if the DNA cannot be repaired in time [4]. However, if there is loss of resonance in the transfer of photon energy to the system, bacterial regrowth can occur [4].

3.5.2. Bacteria inactivation studies under visible light irradiation

Visible light effect on E. coli assays are shown in Fig. 8 (b). The E. coli assay only saw some inactivation under the low radiation visible light exposure with 12% cell inactivation after 4 h. This may be an indication that with higher dosage of visible light irradiation, passable structural damage will compromise cell viability [4]. The effects of TiO_2 photocatalyst on E. coli was slow in the beginning with an inactivation rate of just 6.3% at 1 h. This then shot up to ~ 75% inactivation after 2 h and then a slight reduction was seen after 3 h. Inactivation rate was ~ 78% after 4 h. It may seem that not enough ROS is produced to facilitate the photocatalytic activity. Coliform inactivation with Ag- doped titania under visible light recorded ~ 99% inactivation after 4 h of exposure time. Since

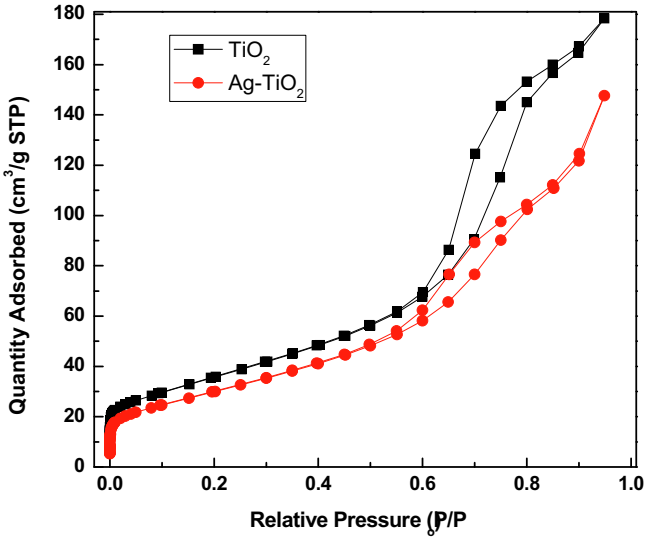

Fig. 6. N_2 adsorption/desorption isotherms of 450 °C calcined TiO_2 and Ag-doped TiO_2.

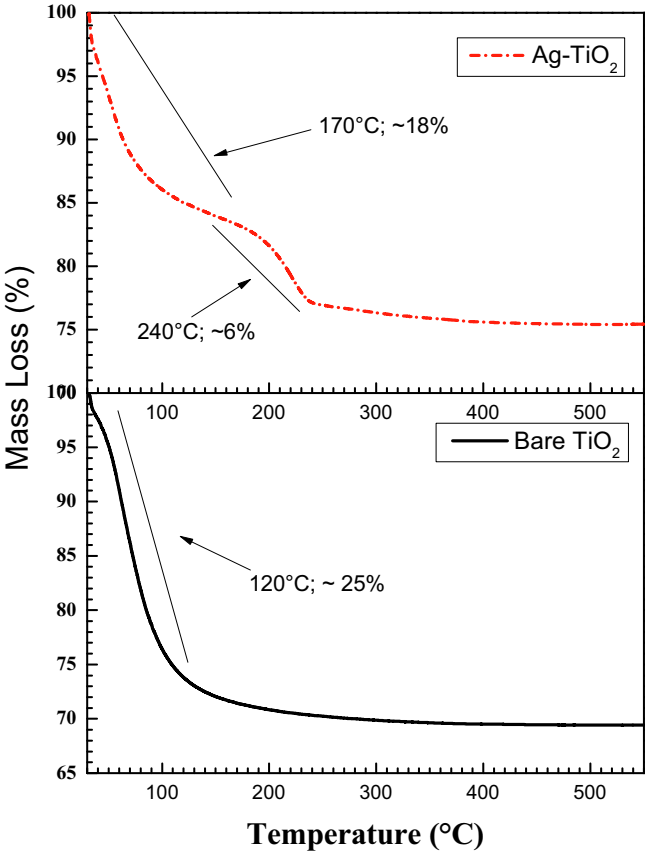

Fig. 7. TGA of As-prepared Ag-TiO_2 and TiO_2.

Ag is known to have bactericidal properties [14], there was a synergistic effect with the photocatalysis process. The Ag is able to enhance the photocatalytic abilities of TiO_2 because of the surface plasmonic resonance effect which causes the shift of bands into the visible absorbance region [16]. The release of Ag^+ ions sets electron traps, reducing the photo-induced charge carriers (electron-hole pair) recombination kinetics and thus increases production of ROS, and subsequent photocatalytic efficiency [14]. Work done by Wu et al. in studying the visible light-induced bactericidal activity of TiO_2 co-doped with nitrogen and silver established that Ag ions are not solely responsible for bacterial inactivation but rather the biocidal effect on bacteria is a combined process of photocatalysis and bactericidal properties of Ag [31]. Another work by Tong-Shong et al. [32], demonstrated that Ag in Montmorillonite-supported titania was not responsible for biocidal effect on bacteria under visible light irradiation.

3.5.3. Bacteria inactivation studies under dark condition

The effect of photocatalyst on bacteria cells in dark condition was investigated. The results can be seen in Fig. 8 (c). Both photocatalysts showed significant bacterial inactivation. Slightly enhanced photoactivity showed by the pristine titania nanoparticles is attributed to the adsorption of bacteria on TiO_2 surfaces. After 4 h, inactivation rate was recorded at ~ 63%. The adsorption onto bacteria cells facilitates the blocking of nutrient intake and passage of waste, eventually leading to cell death [33]. Also, size difference, with the E. coli cells being smaller than the nanoparticles implies that surface to volume ratio is increased. This would mean that nutrient and waste transfer between the cells and their surrounding would occur at fast rates and cause mortality [33]. Ag-doped titania, recorded inactivation rate of 50% after just 1 h. There was a sustained increase and ~ 99% inactivation rate after 4 h. The mechanisms of antibacterial effect of silver is still a scientific debate; however, the generally held view is that, upon bacterial/Ag-NPs contact, Ag-NPs are oxidized into Ag^+ by respiratory enzymes [34]. The released Ag^+ ions then bind to the negatively charged peptidoglycan cell wall. Specifically, the Ag^+ ion binds with the purine and pyrimidine base pairs, rupturing the H-bonds in the base pairs, resulting in DNA disruption, leading to cell death [34]. Additionally, the ROS-mediated oxidative stresses also facilitate bacterial cell death [17,29].

4. Conclusion

Doped and undoped nanostructured TiO_2 (anatase) photocatalysts with improved photocatalytic bacterial inactivity were successfully synthesized via a sol–gel route followed by calcination. The addition of Ag^+ ions during the hydrolysis/condensation of the $Ti^{(IV)}$ precursor ensured the doping of TiO_2, leading to the formation of oxygen vacancies as well as Ag^{n+} ions, evenly dispersed in the titania surface matrix. The photocatalytic bacteria inactivation investigations employing the ATCC 15,597 Escherichia coli (E. Coli) strain showed that the $Ag^{n+/0}$ sites act as effective electron acceptors, improving the quantum yields of the production of reactive oxygen species. The biocidal effect of Ag in conjunction with the induced adsorptive stresses of the titania greatly influenced the bacterial inactivation. As a result, the bacteria substrate was efficiently degraded under light conditions, with percentage inactivation of ~ 99% and ~ 97% for Ag-TiO_2 and TiO_2 respectively. These synthesized TiO_2 nanoparticles have potential applications in the light aided decomposition of a wide range of bacteria pollutants. This approach can also be easily adapted to other metallic ion doping agents and different oxides with improvements in the metal loading as efficient materials for photocatalytic applications.

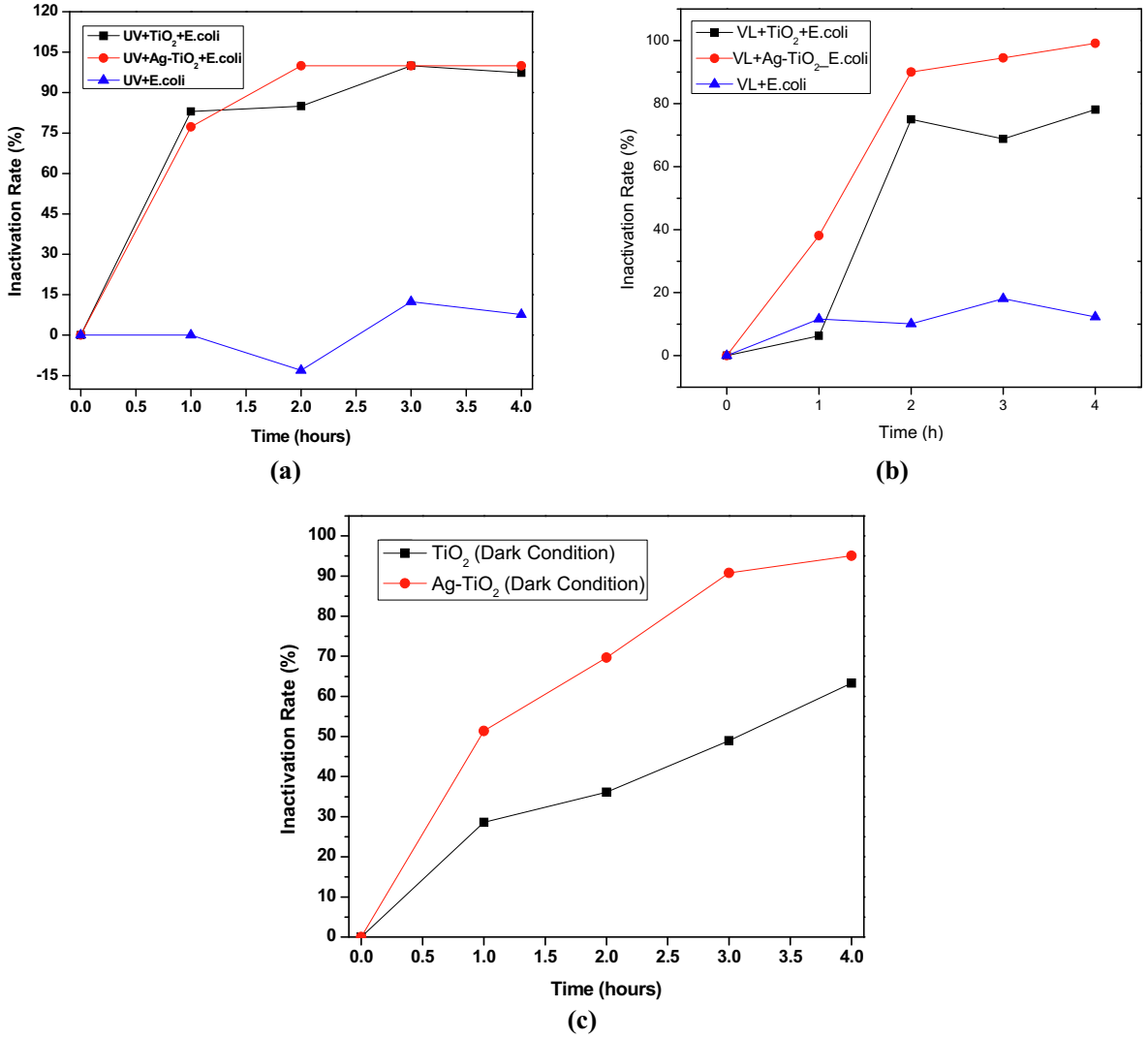

Fig. 8. E. coli Photocatalytic Inactivation under (a) UV-A irradiation, (b) visible light irradiation and (c) dark condition.

CRediT authorship contribution statement

David Dodoo-Arhin: Supervision, validation, Writing - review & editing. **Elsie Bowen-Dodoo:** Supervision, validation, Writing - review & editing. **Benjamin Agyei-Tuffour:** Supervision, validation, Writing - review & editing. **Emmanuel Nyankson:** Supervision, validation, Writing - review & editing. **John D. Obayemi:** Supervision, validation, Writing - review & editing. **Ali A. Salifu:** Supervision, validation, Writing - review & editing. **Abu Yaya:** Supervision, validation, Writing - review & editing. **Henry Agbe:** Supervision, validation, Writing - review & editing. **Winston O. Soboyejo:** Supervision, validation, Writing - review & editing.

Declaration of Competing Interest

The authors declare that they have no known competing financial interests or personal relationships that could have appeared to influence the work reported in this paper.

Acknowledgement

The authors acknowledge support from the University of Ghana BANGA-Africa programme, the Pan-African Materials Institute (PAMI), the African Materials Science and Engineering Network (AMSEN) and the Regional Initiative on Science and Education (RISE).

References

[1] P. J. R. Webb, M. Iskandarani, ZEF Discussion Papers on Development Policy, 2 (1998),1-54.
[2] S. Ramachandran, B. Yamasani, S. Palpandian, S. Bhaskaran, S. Dhanasekar, S. Ethirajulu, Int. J. Med. Sci. Public Heal. 6 (12) (2017) 1718–1721.
[3] J. Lipson, L. Anderson, S. Bolton, EPAR Tech. Rep. 104 (2010) 1–20.
[4] N. Vermeulen, W.J. Keeler, K. Nandakumar, K.T. Leung, Biotechnol. Bioeng. 99 (3) (2008) 550–556.
[5] L. Macdonald, Household Water Treatment and Safe Storage in Ghana: An Interim Solution? PhD thesis, Johns Hopkins University, 2017, p 259.
[6] A.O. Ibhadon, P. Fitzpatrick, Catalysts 3 (2013) 189–218.
[7] R. Saravanan, F. Gracia, and A. Stephen. in M. M. Khan, D. Pradhan, Y. Sohn (eds), Nanocomposites for Visible Light-induced Photocatalysis," Springer Series on Polymer and Composite Materials book series (SSPCM), Switzerland, 2017, pp. 19–41.
[8] P.V. Laxma Reddy, B. Kavitha, P.A. Kumar Reddy, K.H. Kim, Environ. Res. 154 (2017) 296–303.
[9] R. Fagan, D.E. McCormack, D.D. Dionysiou, S.C. Pillai, Mater. Sci. Semicond. Process 42 (2016) 2–14.
[10] I. Capek, Nanocomposite structures and dispersions, (1st Ed.),., Elsevier Science, 2006, pp. 1–69.
[11] Ralf Riedel, I-Wei Chen, Ceramics Science and Technology: Materials and Properties, vol. 2, Wiley Ceramics Science and Technology (VCH), 2010
[12] S. Singh, Development of Novel Polystyrene supported TiO_2 Photocatalysts for Dye Wastewater Treatment PhD thesis, Jaypee University of Engineering and Technology, Guna, 2007, pp. 9–65.

[13] J. Moma and J. Baloyi," Intech open, 2 (2018) 64
[14] K. Venkateswarlu, M. Harikishore, M. Sandhyarani, T.A. Nellaippan, N. Rameshbabu, Procedia Mater. Sci. 6 (2014) 557–566.
[15] V. Etacheri, C. Di Valentin, J. Schneider, D. Bahnemann, S.C. Pillai, J. Photochem. Photobiol. C Photochem. Rev. 25 (2015) 1–29.
[16] H. A. R. A. Ra'ouf Ahmed, ''Preparation and Characterization of Copper-Doped and Silver-Doped Titanium Dioxide Nano-Catalysts," Theses, United Arab Emirates University, 2015
[17] S.L. Percival, A.-M. Salisbury, R. Chen, Crit Rev Microbiol. 45[2] (2019) 223–237.
[18] K. Gupta, R.P. Singh, A. Pandey, A. Pandey, Beilstein J. Nanotechnol. 4 (1) (2013) 345–351.
[19] T. Sakthivel, K. Jagannathan, Mech. Mater. Sci. Eng. 4 (2017) 2412–5954.
[20] M. Ozimek, M. Palewicz, A. Hreniak, Acta Phys. Pol. A 129 (6) (2016) 1214–1219.
[21] S. Thomas, S. K. Nair, E. M. A. Jamal, S. H. Al-Harthi, M. R. Varma, and M. R. Anantharaman, Nanotechnology, 19[7] (2008) 075710
[22] X. B. Chen, Y. B. Lou, A. C. S. Samia, C. Burda and J. L. Gole, Adv. Funct. Mater., 15 [1] (2005) 41–49.
[23] M.C. Mathpal, A.K. Tripathi, M.K. Singh, S.P. Gairola, S.N. Pandey, A. Agarwal, Chem. Phys. Lett. 555 (2013) 182–186.
[24] M.N. Iliev, V.G. Hadjiev, A.P. Litvinchuk, Vib. Spectrosc. 64 (2013) 148–152.
[25] H. Fang, C.X. Zhang, L. Liu, Y.M. Zhao, H.J. Xu, Biosens. Bioelectron 64 (2015) 434–441.
[26] J.C. Parker, R.W. Siegel, Appl. Phys. Lett. 57 (1990) 943–945.
[27] C.A. Melendres, A. Narayanasamy, V.A. Maroni, R.W. Siegel, J. Mater. Res. 4[5] (1989) 1246–1250.
[28] J.C. Parker, R.W. Siegel, J. Mater. Res. 5[6] (1989) 1246–1252.
[29] E.-Y. Kim, D. S. Kim, and B.-T. Ahn, Bull. Korean Chem. Soc., 30[1] (2009) 193-196.
[30] M. Li et al., Environ. Sci. Technol., 45[20] (2011) 8989–8995
[31] K. I. and J.-K. S. Pinggui Wu, Rongcai Xie, Environ. Sci. Technol., 44[18] (2010) 6992–6997.
[32] T.S. Wu, K.X. Wang, G.D. Li, S.Y. Sun, J. Sun, J.S. Chen, A.C.S. Appl, Mater. Interfaces 2 (2) (2010) 544–550.
[33] A. Erdem, D. Metzler, D.K. Cha, C.P. Huang, Environ. Sci. Pollut. Res. 22 (22) (2015) 17917–17924.
[34] S.L. Banerjee, P. Potluri, N.K. Singha, Colloids Surf., A 566 (2019) 176–187.